Int. J. Solids Structures Vol. 17, pp. 915–924, 1981
Printed in Great Britain. 

0020-7683/81/090915-10$02.00/0


# PENETRATION INTO TARGETS DESCRIBED BY LOCKED HYDROSTATS AND SHEAR STRENGTH†

M. J. FORRESTAL, F. R. NORWOOD and D. B. LONGCOPE
Sandia National Laboratories,‡ Albuquerque, NM 87185, U.S.A.

(*Received* 22 *September* 1980; *in revised form* 17 *November* 1980)

**Abstract**—The penetration of projectiles with conical and ogival nose shapes into target media described by a locked hydrostat and a linear shear failure–pressure relation is investigated. A cylindrical cavity expansion approximation is employed which idealizes the target as thin independent layers normal to the penetration direction and permits one-dimensional wave propagation calculations in the radial coordinate. Closed-form expressions are derived for the stresses on the penetrator nose, stress profiles in the target and the resultant axial force on the penetrator nose.

## INTRODUCTION

Studies concerned with the penetration of projectiles into geological targets usually focus on the depth of penetration, penetrator deceleration history or stresses on the nose. Predictions of these quantities use solution techniques that may be grouped into three main categories: (1) empirical equations for final penetration depth based on test data[1, 2], (2) models which approximate the target response by one-dimensional motion using cylindrical or spherical cavity expansion methods[3–7], and (3) detailed numerical solutions which employ two-dimensional wave codes[8, 9]. All of these approaches have advantages and limitations which must be considered for a given application.

The present study uses the cylindrical cavity expansion approximation which idealizes the target as thin independent layers normal to the penetration direction as shown in Fig. 1. Only radial motion of the target material is permitted, but this should be a reasonable assumption for slender projectiles. In a recent paper[3], the authors utilized this approximation to obtain forces on conical-nosed penetrators for targets described by a linear hydrostat and a linear shear failure–pressure relation. Since many dry sand, grout and rock[10, 11] materials have hydrostats which are initially linear, stiffen and then approach a locking limit with increasing hydrostatic pressure, solutions for locked hydrostats (Fig. 2) are also of interest. For a specified target and penetrator, the penetrator velocity determines the state on the hydrostat, and for sufficiently high velocity locking solutions are applicable. Thus, formulas derived in this study for a locked hydrostat complement the results of[3] for a linear hydrostat.

Previous studies on penetration into targets with locked hydrostats calculate stresses on the penetrator nose and use a constant shear failure–pressure relation[4] or a perturbation method to model soft soil with small shear strength[5]. This study uses a linear shear failure description for the target and results for the constant shear failure relationship are included as special cases. In addition, closed-form expressions for projectiles with conical and ogival nose shapes are derived for stresses on the penetrator nose, stress-profiles in the target and the axial resultant force.

## FORMULATION OF THE PROBLEM

A rigid projectile with a conical or ogival nose penetrates a uniform target medium with normal incidence. The problem is axisymmetric and is further simplified by applying the cylindrical cavity expansion approximation. As shown in Fig. 1, this approximation considers the target as thin layers normal to the direction of penetration and simplifies the analysis to one-dimensional wave progagation in the radial coordinate. This model assumes that all motion in individual target layers is one-dimensional, radial and independent of any other layer.

†This work was supported by the U.S. Department of Energy and the U.S. Army, Pershing II Project Manager's Office.
‡A U.S. Department of Energy Facility.

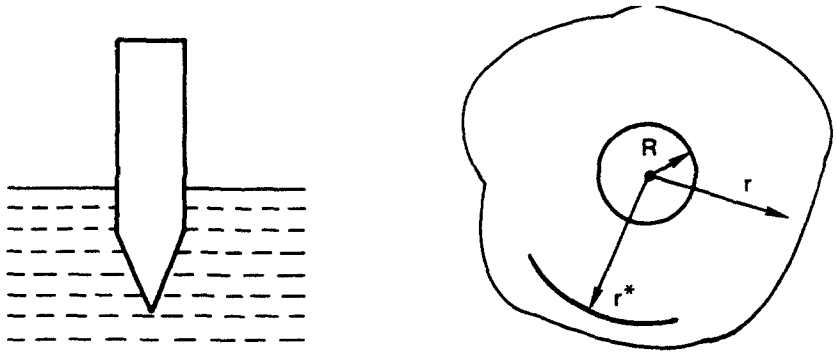


Fig. 1. Geometry for cylindrical cavity expansion.

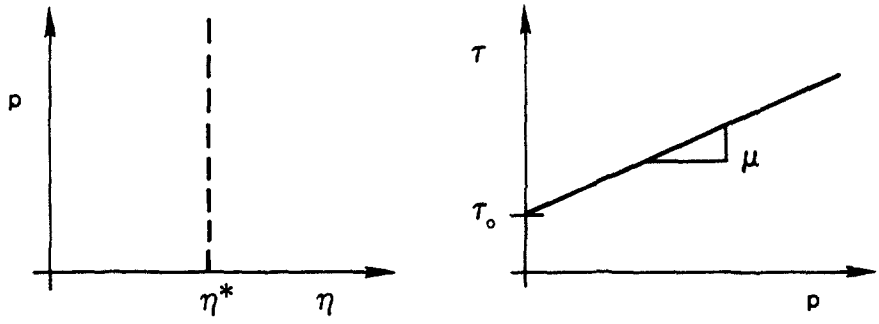


Fig. 2. Material model.

The target medium is described by the locked hydrostat and linear shear failure-pressure relation shown in Fig. 2. It is further assumed that $\sigma_z = \sigma_\theta$ during the penetration event which matches the physical situation for triaxial material tests[10]. Thus, the hydrostatic pressure is given by

$$p = 1/3(\sigma_r + 2\sigma_\theta) \tag{1a}$$

and the shear failure-pressure relation is given by

$$\tau = \sigma_r - \sigma_\theta = \tau_0 + \mu p. \tag{1b}$$

Equations (1a, b) are combined to give the radial stress component

$$\sigma_r = (1 + 2\,\mu/3)\,p + 2\tau_0/3. \tag{1c}$$

An idealized layer of target material is expanded by the penetrator as shown in Fig. 1. The equations of momentum and mass conservation in cylindrical, Lagrangian coordinates[9] are

$$\rho_0 r \frac{\partial^2 u}{\partial t^2} = -(r+u)\frac{\partial \sigma_r}{\partial r} - (\sigma_r - \sigma_\theta)\frac{\partial}{\partial r}(r+u) \tag{2a}$$

$$\frac{1}{2}\frac{\partial}{\partial r}(r+u)^2 = \frac{\rho_0}{\rho} r \tag{2b}$$

where $\rho_0$, $\rho$ are the initial and current densities, $u$ is the radial displacement and $\sigma_r$, $\sigma_\theta$ are the radial and circumferential components of Cauchy stress, taken positive in compression. Elastic strains are neglected and eqns (1a, b and c) are used to eliminate $\sigma_\theta$ from eqn (2a) which

becomes

$$\rho_0 r \frac{\partial^2 u}{\partial t^2} = -(r+u)\frac{\partial \sigma_r}{\partial r} - \nu\sigma_r \frac{\partial}{\partial r}(r+u) - \frac{\tau_0 \nu}{\mu}\frac{\partial}{\partial r}(r+u) \tag{3a}$$

$$\nu = 3\mu/(3+2\mu). \tag{3b}$$

The nose of the rigid penetrator traveling at constant velocity $V$ begins to open a circular cavity in a given layer at time $t = 0$. Radial displacement at the cavity wall $u(0, t) = R(t)$ is specified by the nose shape. For a conical nose

$$R(t) = (V \tan \phi)\, t. \tag{4a}$$

The ogive shape is an arc of a circle with radius $s$ and is tangent to the cylindrical aft body as shown in Fig. 3. For an ogive nose shape

$$R(t) = (a - s) + [s^2 - (l - z)^2]^{1/2}, \quad z = Vt. \tag{4b}$$

The other boundary condition requires that the radial displacement at the wave front is zero and the formulation of the cavity expansion problem is complete.

## CAVITY EXPANSION SOLUTION†

For the idealized hydrostat shown in Fig. 2., the density at the wave front $\rho = \rho^*$ is the specified locked density. With constant density, eqn (2b) can be integrated to give

$$(r+u)^2 = (1-\eta^*)\, r^2 + R^2(t) \tag{5a}$$

$$\eta^* = 1 - \rho_0/\rho^* \tag{5b}$$

where $R(t)$ is the motion of the cavity wall. Since $u = 0$ at the wave front position $r = r^*$, the wave front location is given by

$$r^* = R/(\eta^*)^{1/2} \tag{5c}$$

where the asterisk indicates wave front values.

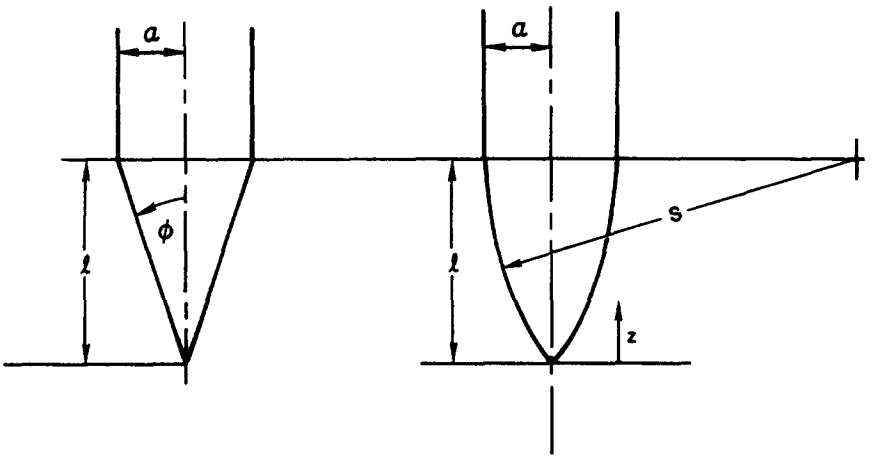


Fig. 3. Conical and ogival nose geometries.

†The solution procedure in this section is similar to that presented in [10] for application to the response of media to long explosive charges.

Mass and momentum conservation equations across the wave front are

$$\dot{u}^* = \dot{r}^* \eta^*, \quad \sigma_r^* = \rho_0 \eta^* (\dot{r}^*)^2 \tag{6}$$

where dot indicates differentiation with respect to time. Differentiation of eqn (5a) with respect to time and evaluation at the wave front gives

$$r^* \dot{u}^* = R\dot{R}. \tag{7}$$

From eqns (5c), (6) and (7) the wave front radial stress and wave front propagation velocity are

$$\sigma_r^* = \rho_0 \dot{R}^2, \quad \dot{r}^* = \dot{R}/(\eta^*)^{1/2}. \tag{8}$$

Multiplying both sides of eqn (3a) by $(r+u)^{\nu-1}$ and integrating with respect to $r$ gives

$$(r+u)^\nu \sigma_r(r) = \rho_0 \int_r^{r^*} (r+u)^{\nu-1} r \frac{\partial^2 u}{\partial t^2} \, dr + (r^*)^\nu \sigma_r^* + (\tau_0/\mu)[(r^*)^\nu - (r+u)^\nu]. \tag{9}$$

Using eqns (5a) and (8) the above equation can be written as

$$\begin{aligned} \sigma_r(r) = {} & \frac{\rho_0(\dot{R}^2 + R\ddot{R})}{(r+u)^\nu} \int_r^{r^*} r[(1-\eta^*) r^2 + R^2]^{(\nu/2-1)} \, dr \\ & - \frac{\rho_0 (R\dot{R})^2}{(r+u)^\nu} \int_r^{r^*} r[(1-\eta^*) r^2 + R^2]^{(\nu/2-2)} \, dr \\ & + \rho_0 \dot{R}^2 [\eta^* + (1-\eta^*)\xi^2]^{-\nu/2} \\ & + (\tau_0/\mu)\{[\eta^* + (1-\eta^*)\xi^2]^{-\nu/2} - 1\} \end{aligned} \tag{10}$$

which integrates to

$$\begin{aligned} \sigma_r(r) = {} & \frac{\rho_0[\dot{R}^2 + R\ddot{R}]}{\nu(1-\eta^*)} \{[\eta^* + (1-\eta^*)\xi^2]^{-\nu/2} - 1\} \\ & + \frac{\rho_0 \dot{R}^2 \eta^*}{(2-\nu)(1-\eta^*)} \{[\eta^* + (1-\eta^*)\xi^2]^{-\nu/2} - [\eta^* + (1-\eta^*)\xi^2]^{-1}\} \\ & + \rho_0 \dot{R}^2 [\eta^* + (1-\eta^*)\xi^2]^{-\nu/2} + (\tau_0/\mu)\{[\eta^* + (1-\eta^*)\xi^2]^{-\nu/2} - 1\} \end{aligned} \tag{11a}$$

in which

$$\xi = r/r^*, \quad r^* = R/(\eta^*)^{1/2}. \tag{11b}$$

For the special case where $\mu = 0$ for a constant shear failure-pressure relation eqn (2a) integrates to

$$\begin{aligned} \sigma_r(r) = {} & \rho_0 \dot{R}^2 \left\{1 - \frac{\eta^*(1-\xi^2)}{2[\eta^* + (1-\eta^*)\xi^2]}\right\} \\ & - \frac{\rho_0(\dot{R}^2 + R\ddot{R})}{2(1-\eta^*)} \ln[\eta^* + (1-\eta^*)\xi^2] \\ & - (\tau_0/2) \ln[\eta^* + (1-\eta^*)\xi^2], \quad \text{for } \mu = 0 \end{aligned} \tag{12}$$

These eqns (11a) and (12) for radial stress indicate that the contribution due to $\tau_0$ is independent of the nose shape.

Equations (11) and (12) give the radial stress in the annulus between the cavity wall specified by $R(t)$ and the wave front radius $r^*$. The nose shapes specify $R(t)$ and are given by eqns (4a, b). For the conical nose

$$\dot{R}^2 = (V\tan\phi)^2, \quad \ddot{R} = 0 \tag{13}$$

and for the ogival nose

$$\dot{R}^2 = \frac{V^2(l-z)^2}{s^2-(l-z)^2}, \quad z = Vt \tag{14a}$$

$$\dot{R}^2 + R\ddot{R} = -V^2\left\{1 - \frac{s^2(s-a)}{[s^2-(l-z)^2]^{3/2}}\right\}. \tag{14b}$$

The radial stress component on the penetrator nose can be determined from eqns (11) or (12) with $\xi = 0$ and eqns (13) and (14). If, however, the radial nose stress becomes tensile, the target medium will separate from the penetrator nose.

## NOSE STRESSES AND AXIAL RESULTANT FORCES

The radial stress on a conical nose are obtained from eqns (11), (12) and (13) and are given by

$$\sigma_r(0) = \frac{\rho_0(V\tan\phi)^2}{(1-\eta^*)(\eta^*)^{\nu/2}}\left[1-\eta^*+\frac{1}{\nu}+\frac{\eta^*}{2-\nu}\right] \tag{15}$$

$$-\frac{\rho_0(V\tan\phi)^2}{(1-\eta^*)}\left[\frac{1}{\nu}+\frac{1}{2-\nu}\right]+(\tau_0/\mu)\left[(\eta^*)^{-\nu/2}-1\right]$$

and

$$\sigma_r(0) = \frac{\rho_0(V\tan\phi)^2}{2}\left[1-\frac{1}{1-\eta^*}\ln\eta^*\right]-\frac{\tau_0}{2}\ln\eta^*, \quad \text{for } \mu = 0. \tag{16}$$

These results indicate that the stress profiles are constant for a conical nose. The incremental radial ring force for a thin target layer with thickness dz is

$$\mathrm{d}F_r = \sigma_r\,\mathrm{d}A = 2\pi\sigma_r(0)R(z)\,\mathrm{d}z \tag{17}$$

where $\mathrm{d}F_r$ is interpreted as the radial component of the incremental normal force. Thus, the incremental axial force is

$$\mathrm{d}F_z = \mathrm{d}F_r\tan\phi \quad \text{and} \tag{18a}$$

$$F_z = 2\pi\sigma_r(0)\int_0^l z\tan^2\phi\,\mathrm{d}z = \pi a^2\sigma_r(0) \tag{18b}$$

where $a$ is the radius of the cylindrical portion of the penetrator shown in Fig. 3 and $\sigma_r(0)$ is given by eqn (15) or (16).

The radial stresses on an ogival nose are obtained from eqns (11) and (12) and are

$$\sigma_r(0) = \rho_0\dot{R}^2\left[(\eta^*)^{-\nu/2}-\frac{(\eta^*)^{1-\nu/2}-1}{(1-\eta^*)(\nu-2)}\right]$$

$$+\frac{\rho_0(\dot{R}^2+R\ddot{R})}{\nu(1-\eta^*)}\left[(\eta^*)^{-\nu/2}-1\right]+(\tau_0/\mu)\left[(\eta^*)^{-\nu/2}-1\right] \tag{19}$$

and

$$\sigma_r(0) = \frac{\rho_0 \dot{R}^2}{2} - \frac{\rho_0(\dot{R}^2 + R\ddot{R}) \ln \eta^*}{2(1-\eta^*)} - \frac{\tau_0}{2} \ln \eta^*, \quad \text{for } \mu = 0 \tag{20}$$

where $\dot{R}$ and $(\dot{R}^2 + R\ddot{R})$ are given by equations (14a, b). The axial resultant force on an ogival nose is

$$F_z = 2\pi \int_0^{\lambda} \sigma_r(0)\, R \cdot \frac{dR}{dz}\, dz \tag{21}$$

where $dR/dz$ replaces $\tan \phi$ in eqn (18a) and the upper limit of integration $\lambda$ corresponds to the axial position where the radial stress becomes tensile and the target is no longer in contact with the penetrator. Substitution of eqns (4b) and (19) into eqn (21) and performing the integration gives

$$F_z = 2\pi\rho_0 V^2 C_1 \left[ (\eta^*)^{-\nu/2} - \frac{(\eta^*)^{1-\nu/2} - 1}{(\nu-2)(1-\eta^*)} \right]$$

$$- 2\pi\rho_0 V^2 C_2 \left[ \frac{(\eta^*)^{-\nu/2} - 1}{\nu(1-\eta^*)} \right] + 2\pi \frac{\tau_0}{\mu} C_3 [(\eta^*)^{-\nu/2} - 1] \tag{22}$$

where the constants $C_1$, $C_2$ and $C_3$ are given by

$$C_1 = \frac{l^2}{2} + \frac{(l-\lambda)^2}{2} - 2s^2 + [2s^2 - (l-\lambda)^2] \left[ \frac{s^2 - l^2}{s^2 - (l-\lambda)^2} \right]^{1/2}$$

$$- \frac{s^2}{2} \ln \left[ \frac{s^2 - l^2}{s^2 - (l-\lambda)^2} \right] \tag{23a}$$

$$C_2 = -\frac{l^2}{2} - \frac{(1-\lambda)^2}{2} + \frac{s^2}{2} + s^2 \left[ \frac{s^2 - l^2}{s^2 - (l-\lambda)^2} \right]^{1/2} \tag{23b}$$

$$- (s^2 - l^2)^{1/2} [s^2 - (l-\lambda)^2]^{1/2} - \frac{s^2(s^1 - l^2)}{2[s^2 - (l-\lambda)^2]}$$

$$C_3 = -\frac{l^2}{2} - \frac{(l-\lambda)^2}{2} + s^2 - (s^2 - l^2)^{1/2} [s^2 - (l-\lambda)^2]^{1/2}. \tag{23c}$$

For $\mu = 0$, the axial force is given by

$$F_z = \pi\rho_0 V^2 C_1 + \pi\rho_0 V^2 C_2 \frac{\ln \eta^*}{(1-\eta^*)} - \pi\tau_0 C_3 \ln \eta^*. \tag{24}$$

As discussed in (3), acceleration-time can be measured in field tests. If the axial velocity $V$ varies with time, the equation for rigid body motion of a penetrator with mass $m$ is given by

$$m \frac{dV}{dt} = -(AV^2 + B) \tag{25}$$

where $A$, $B$ are given by eqns (15), (16) and (18b) for a conical nose and eqns (22) and (24) for an ogival nose. Equation (25) with the initial condition $V(t=0) = V_0$ has solutions

$$X = \frac{m}{A} \ln \left\{ \frac{\cos[\tan^{-1} V_0/c - Act/m]}{\cos[\tan^{-1} V_0/c]} \right\} \tag{26a}$$

$$V = c \tan[\tan^{-1} V_0/c - Act/m] \tag{26b}$$

$$\frac{dV}{dt} = -B/m \sec^2[\tan^{-1} V_0/c - Act/m] \tag{26c}$$

for distance, velocity and acceleration, where $c = \dot{r}^*$, the wave front velocity.

## NUMERICAL RESULTS AND DISCUSSION

Some numerical results for a conical-nosed penetrator are presented in Figs. 4–6. Radial stress profiles in the target are shown in Fig. 4 for several values of $\mu$ and $\tau_0 = 0$.

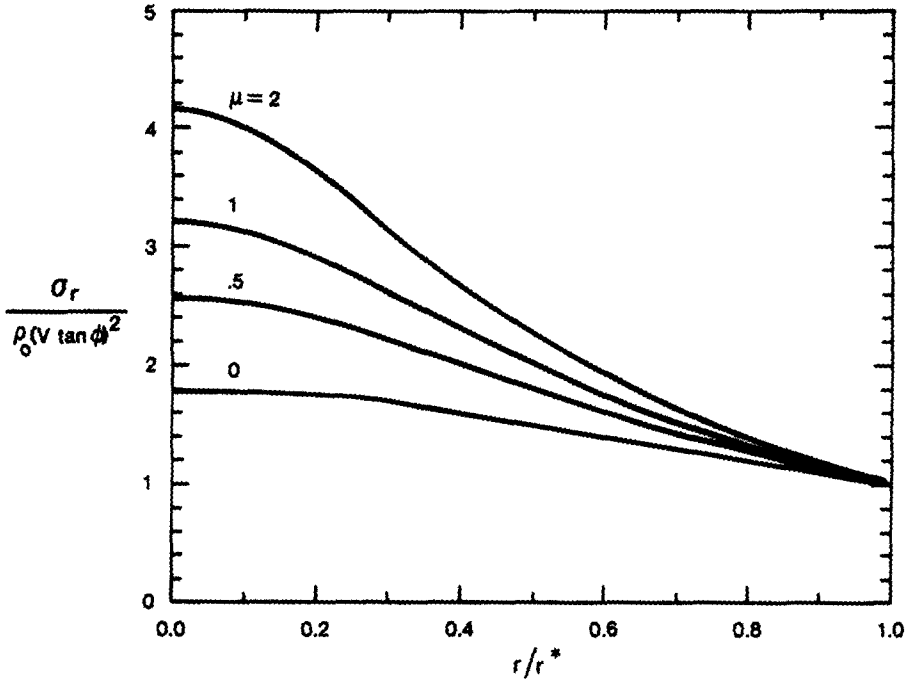


Fig. 4. Radial target stress profiles for a conical nose; $\eta^* = 0.10$, $\tau_0 = 0$.

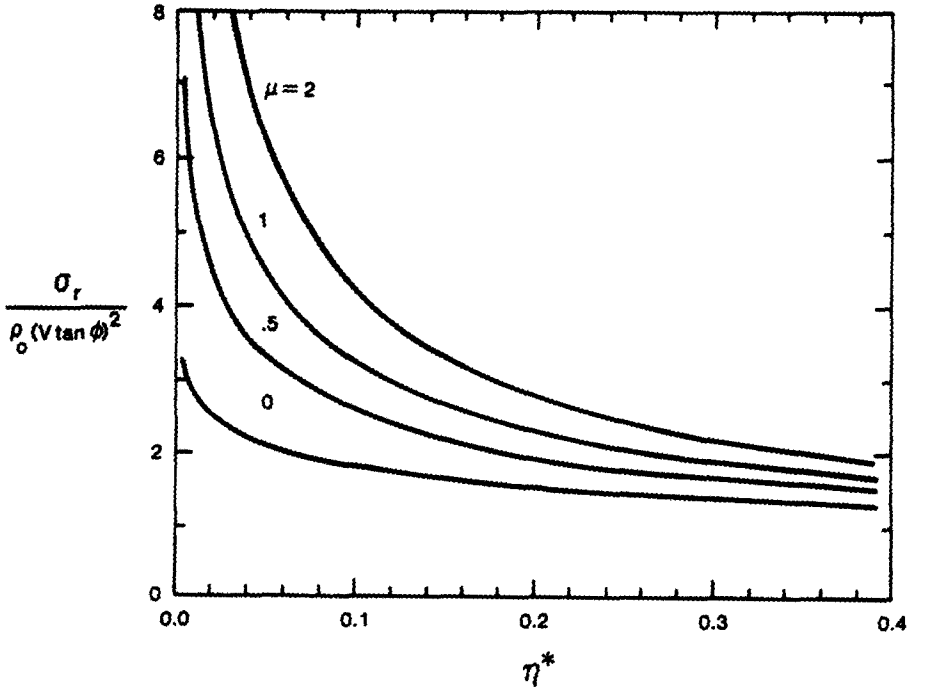


Fig. 5. Radial stress on a conical nose for $\tau_0 = 0$.

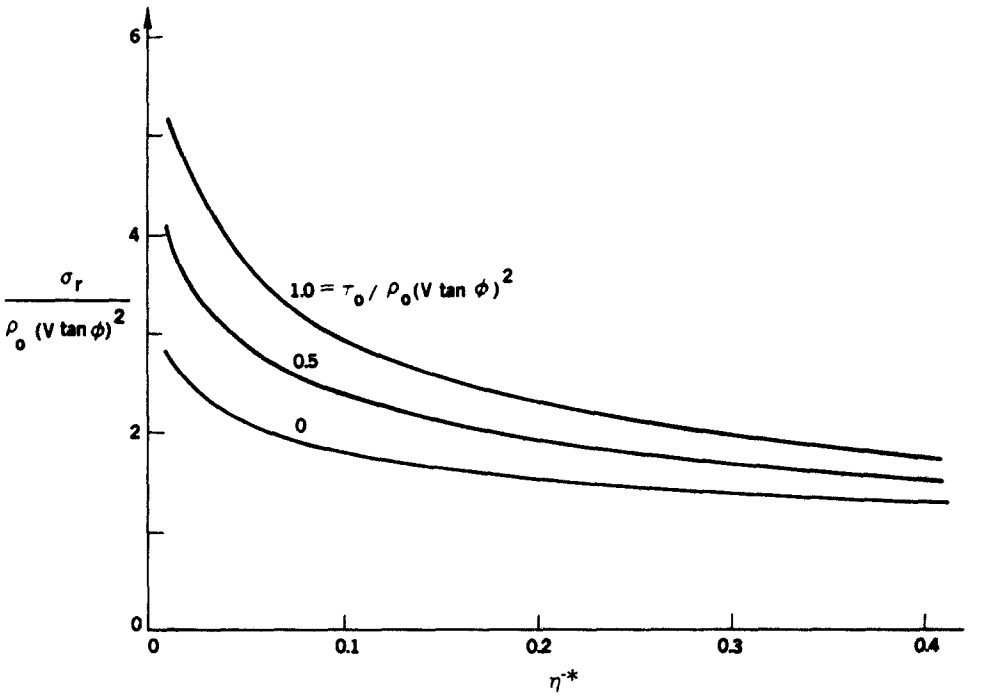


Fig. 6. Radial stress on a conical nose for $\mu = 0$.

These curves show the radial stress increasing behind the wave front and maximum at the penetrator nose. The last term in eqn (11a) indicates that for $\tau_0 \neq 0$ the wave front values remain unchanged and that the contribution in radial stress due to $\tau_0$ monotonically increases from the wave front to the conical nose. Thus, radial stress increases behind the wave front and is maximum at the penetrator surface, $r = 0$, for all values of $\mu$ and $\tau_0$.

Radial stresses on the conical nose vs locked density are shown in Fig. 5 for several values of $\mu$ with $\tau_0 = 0$ and in Fig. 6 for several values of $\tau_0$ with $\mu = 0$. Some criterion for the admissible ranges of $\mu$ and $\tau_0$ is required for this theory. We arbitrarily choose to keep $\sigma_\theta$ compressive† and the parametric ranges in Figs. 5 and 6 reflect this criterion. From equations (1a, b)

$$\sigma_\theta = \left(\frac{3-\mu}{3+2\mu}\right)\sigma_r - \left(\frac{3}{3+2\mu}\right)\tau_0. \tag{27}$$

For $\tau_0 = 0$, the requirement that $\sigma_\theta$ be compressive implies that $\mu \leq 3$, which represents a practical range[3]. With $\mu = 0$, $\sigma_r \geq \tau_0$; and since radial stress is minimal at the wave front given by eqns (8) and (13), $\tau_0 \leq \rho_0 (V \tan\phi)^2$. As previously discussed, radial stress is spatially constant on a conical nose and the resultant axial force can be obtained from eqn (18b).

Numerical results for an ogival nosed penetrator are given in Figs. 7 and 8. The spatial distribution of radial stress on a CRH = 6 (caliber radius head) where

$$\text{CRH} = s/2a \tag{28}$$

is given in Fig. 7 for several values of $\mu$. For these cases with $\tau_0 = 0$, the radial stress becomes tensile in the vicinity of $z \simeq l/2$ which is interpreted as the position where the target separates from the penetrator. As indicated by eqn (19), the inclusion of $\tau_0$ would translate these curves upward and move the position of separation towards the aft cylindrical body. If $\tau_0$ is sufficiently large, no separation on the nose will occur. The resultant axial force versus $\eta^*$ for several values of $\mu$ with $\tau_0 = 0$ is presented in Fig. 8.

†For materials where $\sigma_\theta$ has tensile strength this criterion can be easily modified.

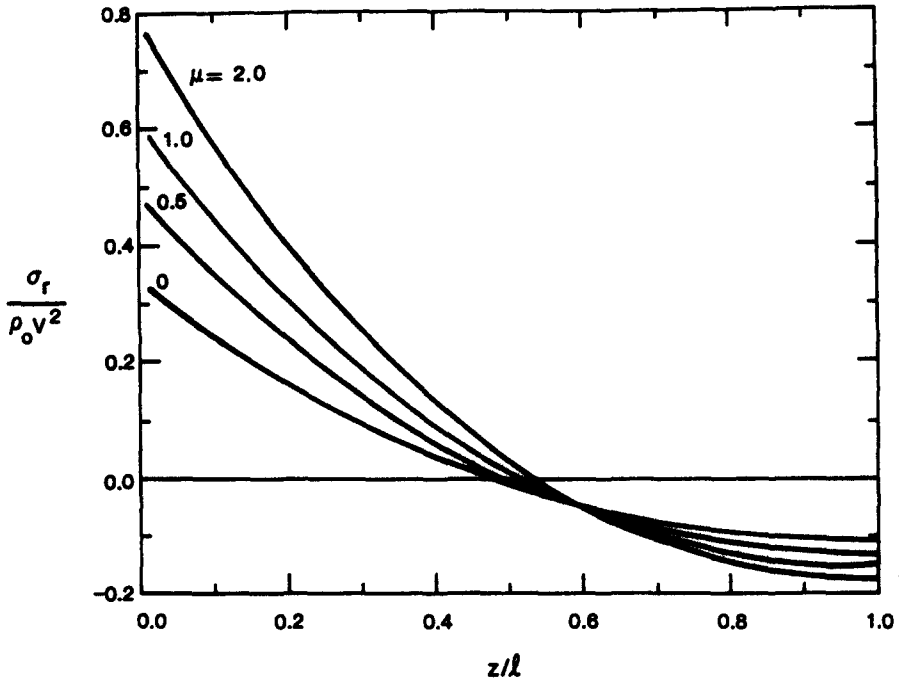


Fig. 7. Radial stress distribution on an ogival nose; CRH = 6, $a$ = 76.2 mm (3.0 in), $\eta^* = 0.10$, $\tau_0 = 0$.

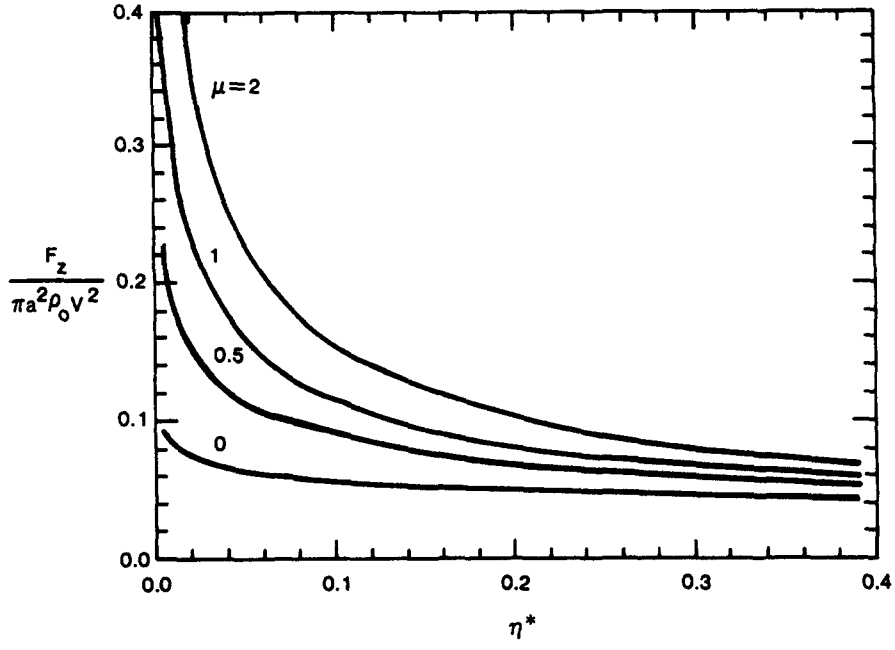


Fig. 8. Resultant axial force on an ogival nose; CRH = 6, $a$ = 76.2 mm (3.0 in), $\tau_0 = 0$.

As previously mentioned, the authors have calculated the forces on a conical-nosed penetrator for targets described by a linear hydrostat and a linear shear failure–pressure relation with $\tau_0 = 0$[3]. Results in[3] indicate that the resultant force on a conical nose is nearly proportional to $V \tan \phi$; whereas, the solutions presented herein for a locked hydrostat predict the resultant force on a conical nose to be proportional to $(V \tan \phi)^2$.

## REFERENCES

1. C. W. Young, Depth prediction for earth penetrating projectiles. *J. Soil Mechanics and Foundation Div. of ASCE* 803–817 (May 1969).
2. R. S. Bernard, Depth and motion prediction of earth penetrators. *Tech. Rep. S-78-4*. U.S. Army Engineer Waterways Experiment Station, Vicksburg, Miss. (June 1978).
3. M. J. Forrestal, D. B. Longcope and F. R. Norwood, A model to estimate forces on conical penetrators into hard geological targets. *J. Appl. Mech.*, Vol. 48, March 1981, pp. 25–29.
4. F. R. Norwood, Cylindrical cavity expansion in a locking soil. *SLA-74-0201*, Sandia Laboratories, Albuquerque (July 1974).
5. P. Yarrington, A one-dimensional approximate technique for earth penetration calculations. *SAND* 77-1126, Sandia Laboratories, Albuquerque (Sept. 1977).
6. J. N. Goodier, On the mechanics of indentation and cratering in solid targets of strain-hardening metal by impact of hard and soft spheres. *Proc. 7th Symp. on Hypervelocity Impact*, Vol. III, pp. 215–259 (1965).
7. N. T. Davie, A method for describing nearly normal penetration of an ogive nosed penetrator into terrestial targets. *SAND* 79-0721, Sandia Laboratories, Albuquerque, (June 1979).
8. R. K. Byers, P. Yarrington and A. J. Chabai, Dynamic penetration of soil media by slender projectiles. *Int. J. Engng. Sci.* 16, 835–844 (1978).
9. M. H. Wagner, C. C. Fulton and K. N. Kreyenhagen, Finite-difference code analyses of earth penetrator dynamics in rock media. *DNA* 4069T, California Research and Technology, Inc., Woodland Hills, California (Nov. 1976).
10. N. Christescu, *Dynamic Plasticity*, Chapt. IX. North-Holland, Amsterdam (1967).
11. S. W. Butters, A. H. Jones and R. K. Dropek, Material properties of Nevada test side tuff and grout with emphasis on the mighty epic event. *DNA* 4235F, Terra Tek Inc., Salt Lake City, Utah (Nov. 1976).